Three-coordinate copper(I) amido and aminyl radical complexes

Neal P. Mankad, William E. Antholine, Robert K. Szilagyi, and Jonas C. Peters

Supporting Information

General synthetic considerations. All manipulations were carried out using standard Schlenk or glovebox techniques under a dinitrogen atmosphere. Unless otherwise noted, solvents were deoxygenated and dried by thoroughly sparging with N_2 gas followed by passage through an activated alumina column. Non-halogenated solvents were tested with a standard purple solution of sodium benzophenone ketyl in tetrahydrofuran in order to confirm effective oxygen and moisture removal. All reagents were purchased from commercial vendors and used without further purification unless otherwise stated. Lithium amides were prepared by deprotonation of the corresponding amines with *n*-butyllithium. $[Ph_2BP^{tBu}_2]Cu(pyridine)$[1] and $[FeCp_2][B(3,5\text{-}(F_3C)_2C_6H_3)_4]$ [2] were prepared by literature procedures. Elemental analyses were performed by Desert Analytics, Tucson, AZ. Deuterated solvents were purchased from Cambridge Isotope Laboratories, Inc., degassed, and dried over activated 3-Å molecular sieves prior to use.

NMR measurements. A Varian Mercury-300 spectrometer was used to record ^1H, ^{13}C, and ^{31}P NMR spectra at ambient temperature. ^1H and ^{13}C chemical shifts were referenced to the residual solvent peaks. ^{31}P chemical shifts were referenced to external phosphoric acid (δ = 0 ppm).

Synthesis of $\{[Ph_2BP^{tBu}_2]Cu(NTol_2)\}\{Li(12\text{-crown-}4)_2\}$ (1). $[Ph_2BP^{tBu}_2]Cu(pyridine)$ (0.203 g, 0.324 mmol) and $LiNTol_2$ (0.0659 g, 0.324 mmol) were combined in THF (10 mL), giving a clear yellow solution. After stirring for 5 min, 12-crown-4 (0.131 mL, 0.810 mmol) was added. The resulting bright yellow solution was stirred for 0.5 h, and then the solvent was removed *in vacuo*. The residues were triturated with petroleum ether (10 mL), and a yellow powder was collected on a sintered glass frit. Subsequent washes with petroleum ether (5 x 5 mL) gave analytically pure **1** (0.299 g, 84%). X-ray quality crystals were obtained by slow diffusion of petroleum ether vapors into a concentrated THF solution of **1**. ^1H (THF-d_8, δ): 7.36 (br, 4H, borate *ortho*-C<u>H</u>), 6.8-7.0 (m, 8H, Ar-<u>H</u>), 6.61 (m, 6H, Ar-<u>H</u>), 3.63 (s, 32H, O(C<u>H</u>$_2$)$_2$O), 2.08 (s, 6H, *para*-C<u>H</u>$_3$), 1.46 (br, 4H, BC<u>H</u>$_2$P), 1.01 (d, $^3J_{PH}$ = 5.8 Hz, 18H, P[C(C<u>H</u>$_3$)$_3$]$_2$), 1.00 (d, $^3J_{PH}$ = 5.5 Hz, 18H, P[C(C<u>H</u>$_3$)$_3$]$_2$). $^{13}C\{^1H\}$ (THF-d_8, δ): 162.3 (br, borate *ipso*-<u>C</u>), 156.0 (s, tolyl *ipso*-<u>C</u>), 133.7, 128.4, 125.4, 121.1, 120.4, 69.4 (s, O(<u>C</u>H$_2$)$_2$O), 33.0 (br, P[<u>C</u>(CH$_3$)$_3$]$_2$), 30.2 (P[C(<u>C</u>H$_3$)$_3$]$_2$), 30.1 (P[C(<u>C</u>H$_3$)$_3$]$_2$), 20.3 (s, *para*-<u>C</u>H$_3$), 13.3 (br, B<u>C</u>H$_2$P). $^{31}P\{^1H\}$ (THF-d_8, δ): 30.9 (s). IR (KBr, cm^{-1}): 2914, 2865, 1597, 1491, 1362, 1323, 1290, 1246, 1136, 1098, 1024, 920, 858, 809. Anal. Calcd for $C_{60}H_{96}BCuLiNO_8P_2$: C, 65.36; H, 8.78; N, 1.27. Found: C, 65.22; H, 8.55; N, 1.33.

Synthesis of $[Ph_2BP^{tBu}_2]Cu(NTol_2)$ (2). A solution of $[FeCp_2][B(3,5\text{-}(F_3C)_2C_6H_3)_4]$ (0.230 g, 0.219 mmol) in dichloromethane (12 mL) was added in one portion to solid **1** (0.242 g, 0.219 mmol), resulting in a cherry red solution. After stirring for 15 min, the solvent was removed *in vacuo*, leaving a dark red oily residue that was dissolved in petroleum ether (10 mL), filtered through Celite, and allowed to stand at -30°C for 16 h, resulting dark red needles that were crushed and washed thoroughly with petroleum ether to yield analytically pure **2** (41.4 mg, 25%). X-ray quality crystals were obtained by diffusion of hexamethyldisiloxane vapors in a concentrated solution of **2** in petroleum ether at -30°C. IR (KBr, cm^{-1}): 2941, 2865, 1583, 1509, 1474, 1364, 1258, 1154, 1019, 936, 864, 813. Anal. Calcd for $C_{44}H_{64}BCuNP_2$: C, 71.10; H, 8.68; N, 1.88. Found: C, 71.17; H, 8.42; N, 1.85.

Synthesis of [$Ph_2BP^{tBu}_2$]Cu($NHTol_2$) (3). Tributyltin hydride (8.28 μL, 0.0308 mmol) was added to a stirring solution of **3** (21 mg, 0.028 mmol) in benzene (7 mL). After stirring for 4 h, the light yellow solution was concentrated *in vacuo*. The residues were washed thoroughly with petroleum ether (3 x 2 mL), leaving behind **3** as a tan powder (7.8 mg, 37%). The petroleum ether fraction was filtered through alumina and analyzed by GC-MS to reveal the stoichiometric hexabutyldistannane byproduct. Similar results were achieved using 1,2-dihydroanthracene (0.5 eq) or thiophenol in place of tributyltin hydride, yielding anthracene or PhS-SPh (0.5 eq), respectively. Though **3** was isolated in low yield due in part to its petroleum ether solubility, ^{1}H NMR studies established that it was generated quantitatively in the initial reaction mixtures. Attempts to recrystallize **3** from THF/pentane produced the previously characterized [$Ph_2BP^{tBu}_2$]Cu(THF) just as was observed for [$Ph_2BP^{tBu}_2$]Cu(NH_2Mes),[1] and thus far other solvent systems have not yielded crystals suitable for either combustion analysis or X-ray crystallography. Characterization of **3**: ^{1}H (C_6D_6, δ): 7.95 (br, 4H, borate *ortho*-C<u>H</u>), 7.39 (t, J = 6.9 Hz, 4H, borate *meta*-C<u>H</u>), 6.95 (d, J = 8.4 Hz, 4H, tolyl *ortho*-C<u>H</u>), 6.84 (d, J = 8.4 Hz, 4H, tolyl *meta*-C<u>H</u>), 6.73 (t, J = 7.2 Hz, 2H, borate *para*-C<u>H</u>), 4.93 (br s, 1H, N-<u>H</u>), 2.15 (s, 6H, *para*-C<u>H_3</u>), 1.84 (br, 4H, BC<u>H_2</u>P), 1.03 (br, 36H, P[C(C<u>H_3</u>)$_3$]$_2$). ^{13}C{^{1}H} (CD_2Cl_2, δ): 132.9, 130.3, 128.8, 126.9, 126.6, 122.2, 118.1, 34.5 (br, P[<u>C</u>(CH_3)$_3$]$_2$), 30.9 (P[C(<u>C</u>H_3)$_3$]$_2$), 30.3 (P[C(<u>C</u>H_3)$_3$]$_2$), 28.1 (s, *para*-<u>C</u>H_3). ^{31}P{^{1}H} (C_6D_6, δ): 37.7 (br s). IR (C_6H_6, cm^{-1}): 3405 (N-H st), 2922, 2866, 1365, 1293, 1081, 880, 811.

Synthesis of {[$Ph_2BP^{tBu}_2$]Cu(NPh_2)}{Li(12-crown-4)$_2$} (4). A THF solution (8 mL) of lithium diphenylamide (0.050 g, 0.29 mmol) was added to solid [$Ph_2BP^{tBu}_2$]Cu(pyridine) (0.180 g, 0.287 mmol). After stirring for 2 min, 12-crown-4 (0.100 mL, 0.618 mmol) was added by syringe. The resulting cloudy yellow solution was stirred for 12 h, and then volatiles were removed *in vacuo*. Faint yellow residues were washed with pentane (3 x 10 mL) and then recrystallized from THF/pentane (-30ºC). Though combustion analysis of the crystals indicates the formula {[$Ph_2BP^{tBu}_2$]Cu(NPh_2)}{Li(12-crown-4)$_3$}, crushing these crystals and washing with pentane gives a product whose NMR spectroscopy is consistent with the indicated stoichiometry of **4**, i.e. two equivalents of 12-crown-4. Two-crop yield: 0.169 g, 55%. ^{1}H (THF-d_8, δ): 7.36 (br, 4H, borate *ortho*-C<u>H</u>), 6.98 (d, J = 7.5 Hz, 4H, borate *meta*-C<u>H</u>), 6.86-6.75 (m, 8H, amido phenyl *meta*- and *ortho*-C<u>H</u>), 6.62 (t, J = 7.1 Hz, 2H, amido phenyl *para*-C<u>H</u>), 6.18 (t, J = 6.6 Hz, 2H), 3.63 (s, 32H, O(C<u>H_2</u>)$_2$O), 1.48 (br, 4H, BC<u>H_2</u>P), 1.01 (d, $^3J_{PH}$ = 5.4 Hz, 18H, P[C(C<u>H_3</u>)$_3$]$_2$), 0.99 (d, $^3J_{PH}$ = 5.7 Hz, 18H, P[C(C<u>H_3</u>)$_3$]$_2$). ^{13}C{^{1}H} (THF-d_8, δ): 133.7, 132.8, 129.5, 125.4, 121.7, 121.1, 117.3, 69.6 (s, O(<u>C</u>H_2)$_2$O), 33.0 (br, P[<u>C</u>(CH_3)$_3$]$_2$), 30.1 (P[C(<u>C</u>H_3)$_3$]$_2$), 13.5 (br, B<u>C</u>H_2P). ^{31}P{^{1}H} (THF-d_8, δ): 31.0 (s). IR (KBr, cm^{-1}): 3055, 2969, 2918, 2861, 1575, 1478, 1364, 1332, 1313, 1247, 1136, 1098, 1024, 920, 858, 809. Anal. Calcd for $C_{66}H_{108}BCuLiNO_{12}P_2$: C, 63.38; H, 8.70; N, 1.12. Found: C, 63.13; H, 8.62; N, 1.12.

Alternate synthesis of 4. THF (10 mL) was added to the solids **1** (0.345 g, 0.313 mmol) and diphenylamine (0.031 g, 0.33 mmol). The resulting clear, yellow solution was stirred for 12 h, and then volatiles were removed *in vacuo*. The tacky yellow residues were washed with diethyl ether (3 x 10 mL) and dried to yield **4** as an off-white powder (0.223 g, 66%).

Synthesis of {[$Ph_2BP^{tBu}_2$]Cu-N(Ph)C_6H_4}$_2$ (5). A dichloromethane solution (10 mL) of $FeCp_2PF_6$ (0.067 g, 0.20 mmol) was added to solid **4** (0.216 g, 0.201 mmol) in one portion, immediately resulting in a clear, dark red solution. After stirring for 15 min, volatiles were removed *in vacuo*. Diethyl ether (10 mL) was added, the resulting mixture was filtered, and the red filtrate was concentrated *in vacuo* to a red residue. After washing with pentane (10 mL), the remaining tacky red solids were lyophilized from benzene to yield **5** as a dark red powder (0.034 g, 23%). Crystals suitable for X-ray diffraction were grown by diffusion of pentane vapors into a concentrated dichloromethane solution of **5**. Performing the initial stage of the procedure in deuterated dichloromethane and monitoring the reaction *in situ* by NMR

spectroscopy reveals clean and quantitative conversion to **5** and one equiv of $FeCp_2$. However, over a period of 2 days, **5** decomposes to a mixture of unknown colorless species, and hence satisfactory combustion analysis was not obtained. ^{1}H (CD_2Cl_2): 8.00 (d, J = 6.6 Hz, 2H), 7.51 (t, J = 7.5 Hz, 2H), 7.41 (br, 4H, borate *ortho*-C<u>H</u>), 7.35-7.00 (m, 5H), 6.99 (t, J = 7.5 Hz, 4H, borate *meta*-C<u>H</u>), 6.95-6.85 (m, 4H), 6.79 (t, J = 7.2 Hz, 2H, borate *para*-C<u>H</u>), 1.56 (br, 4H, BC<u>H_2</u>P), 1.12 (d, $^3J_{PH}$ = 6.0 Hz, 18H, P[C(C<u>H_3</u>)$_3$]$_2$), 1.10 (d, $^3J_{PH}$ = 5.4 Hz, 18H, P[C(C<u>H_3</u>)$_3$]$_2$). ^{31}P{^{1}H} (CD_2Cl_2, δ): 37.4 (br). IR (KBr, cm^{-1}): 3056, 3040, 2945, 2865, 1590, 1584, 1471, 1427, 1364, 1310, 1180, 1156, 1101, 1018, 937, 862, 812.

Electrochemistry. Electrochemical measurements were carried out in a glovebox under a dinitrogen atmosphere in a one-compartment cell using a CH Instruments 600B electrochemical analyzer. A glassy carbon electrode was used as the working electrode and platinum wire was used as the auxillary electrode. The reference electrode was $Ag/AgNO_3$ in THF. The ferrocene couple Fc^+/Fc was used as an external reference. Solutions (THF) of electrolyte (0.3 M tetra-*n*-butylammonium hexafluorophosphate) and analyte were also prepared under an inert atmosphere.

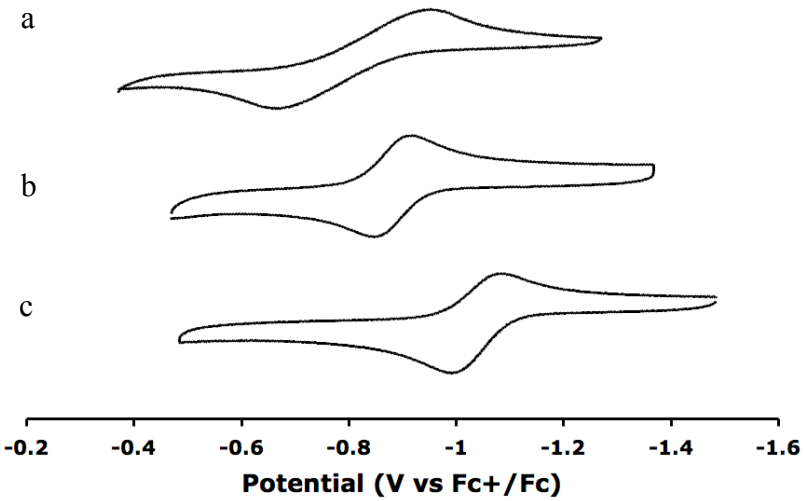

Figure S1. Cyclic voltammograms of (a) $\{[Ph_2BP^{tBu}{}_2]CuNPh_2\}\{Li(12\text{-crown-}4)_2\}$ (**4**), (b) $\{[Ph_2BP^{tBu}{}_2]CuNPh_2\}\{Li(12\text{-crown-}4)_2\}$ (**1**), and (c) $\{[Ph_2BP^{tBu}{}_2]CuNHMes_2\}\{Li(12\text{-crown-}4)_2\}$.[1] Conditions: THF, 0.3 M $[^nBuN_4][PF_6]$ electrolyte, 200 mV/s scan rate.

X-ray Crystallography Procedures. X-ray diffraction studies were carried out at the MIT Department of Chemistry X-Ray Diffraction Facility on a Brüker three-circle Platform diffractometer, equipped with a CCD detector. Data was collected at 100K using Mo Kα (λ = 0.710 73 Å) radiation for all structures and solved using SHELX v. 6.14. X-ray quality crystals were grown as described in the experimental procedures. The crystals were mounted on a glass fiber or nylon loop with Paratone N oil. Structures were determined using direct methods with standard Fourier techniques using the Bruker AXS software package. Disordered solvent and 12-crown-4 regions of **1** and **2** were modeled extensively and restrained using DFIX, SIMU, DELU, and BUMP commands where appropriate.

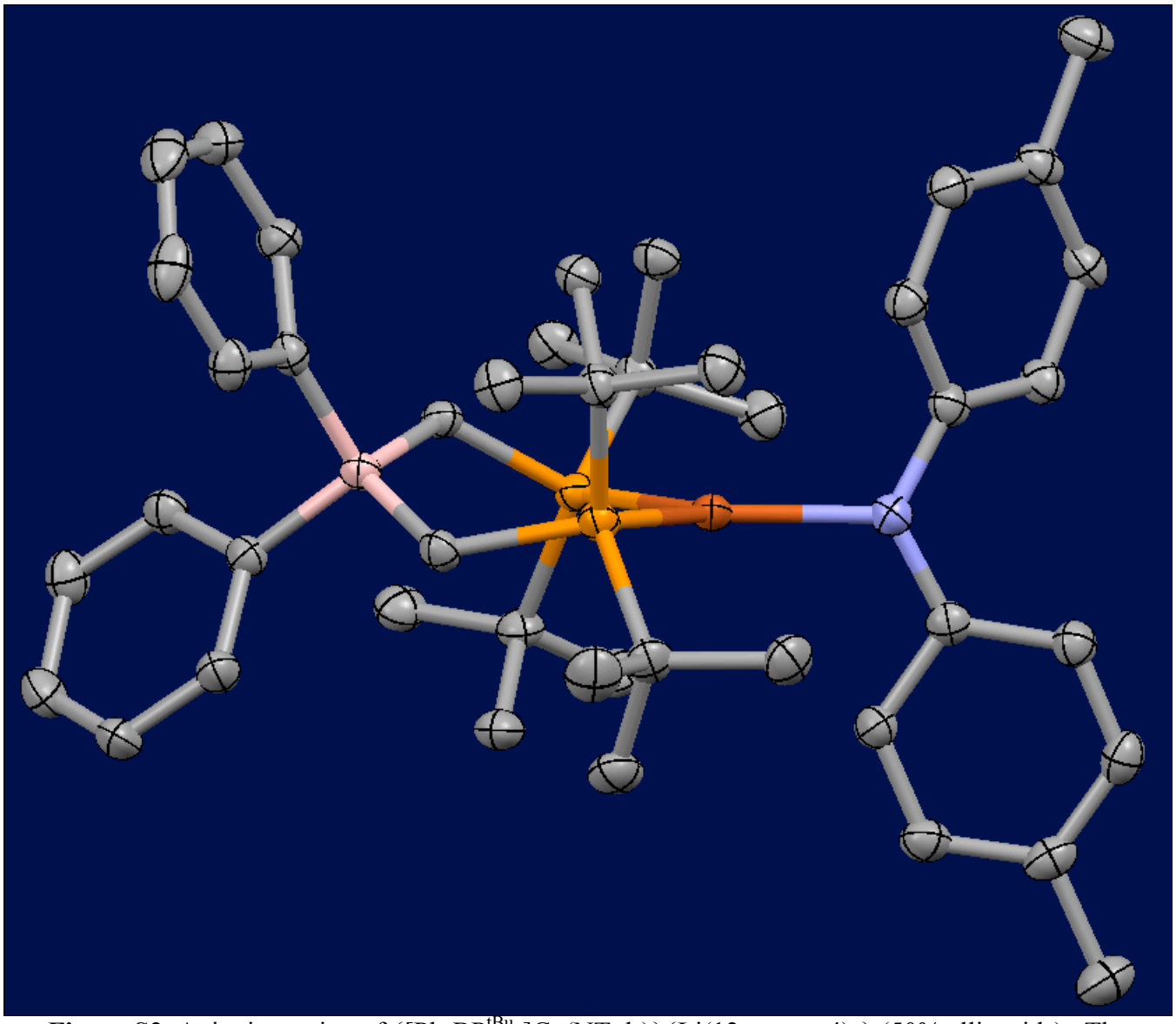

Figure S2. Anionic portion of {[$Ph_2BP^{tBu}_2$]Cu($NTol_2$)}{Li(12-crown-4)$_2$} (50% ellipsoids). The cationic portion, co-crystallized solvent molecules, and hydrogen atoms have been omitted (see CIF file). Cu = red, N = blue, P = orange, B = pink, C = gray.

Table 1. Crystal data and structure refinement for **1**.

Empirical formula	$C_{70.57}H_{118.12}BCuLiNO_{10.02}P_2$	
Formula weight	1284.14	
Temperature	100(2) K	
Wavelength	0.71073 Å	
Crystal system	Triclinic	
Space group	P-1	
Unit cell dimensions	a = 12.9114(9) Å	α = 79.4810(10)°.
	b = 16.8578(12) Å	β = 74.3230(10)°.
	c = 17.6005(12) Å	γ = 80.2250(10)°.
Volume	3596.9(4) $Å^3$	
Z	4	
Density (calculated)	1.186 mg/m^3	
Absorption coefficient	0.403 mm^{-1}	
F(000)	2092	
Crystal size	0.35 x 0.30 x 0.15 mm^3	
Theta range for data collection	1.21 to 29.13°.	
Index ranges	-17<=h<=17, -23<=k<=23, -24<=l<=23	
Reflections collected	78924	
Independent reflections	19261 [R(int) = 0.0564]	
Completeness to theta = 29.13°	99.4 %	
Absorption correction	None	
Refinement method	Full-matrix least-squares on F^2	
Data / restraints / parameters	19261 / 304 / 932	
Goodness-of-fit on F^2	1.015	
Final R indices [I>2sigma(I)]	R1 = 0.0518, wR2 = 0.1274	
R indices (all data)	R1 = 0.0820, wR2 = 0.1458	
Largest diff. peak and hole	0.664 and -0.559 $e.Å^{-3}$	

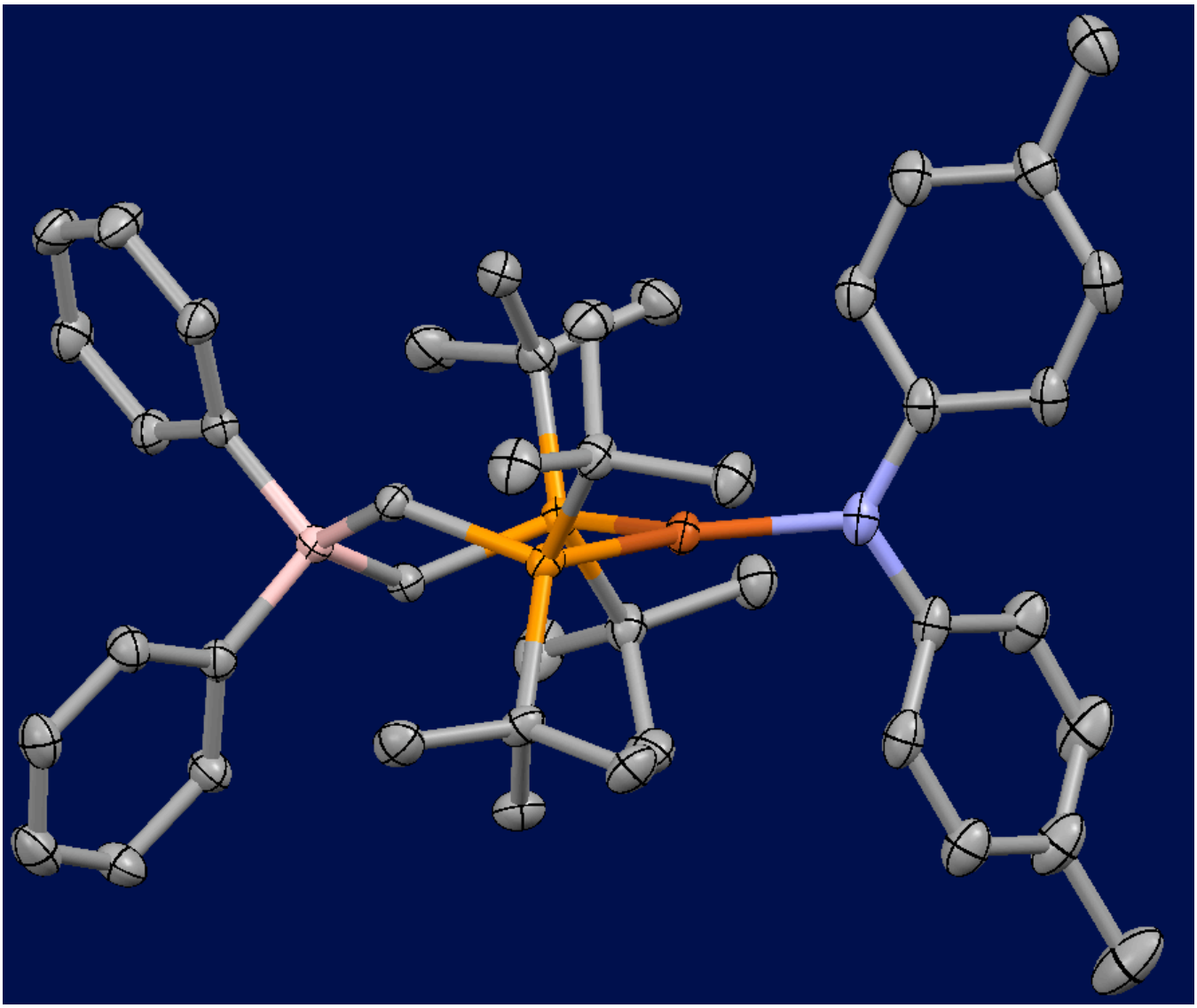

Figure S3. $[Ph_2BP^{tBu}_2]Cu(NTol_2)$ (50% ellipsoids). Co-crystallized solvent molecules and hydrogen atoms have been omitted (see CIF file). Cu = red, N = blue, P = orange, B = pink, C = gray.

Table 2. Crystal data and structure refinement for **2**.

Empirical formula	$C_{52.42}H_{80.84}BCuNP_2$	
Formula weight	861.36	
Temperature	100(2) K	
Wavelength	0.71073 Å	
Crystal system	Monoclinic	
Space group	P2(1)/n	
Unit cell dimensions	a = 16.3201(18) Å	α = 90°.
	b = 16.3538(18) Å	β = 91.277(2)°.
	c = 18.849(2) Å	γ = 90°.
Volume	5029.4(10) $Å^3$	
Z	4	
Density (calculated)	1.137 mg/m^3	
Absorption coefficient	0.531 mm^{-1}	
F(000)	2488	
Crystal size	0.65 x 0.35 x 0.20 mm^3	
Theta range for data collection	1.63 to 29.57°.	
Index ranges	-22<=h<=22, -22<=k<=22, -26<=l<=26	
Reflections collected	132059	
Independent reflections	14110 [R(int) = 0.0613]	
Completeness to theta = 29.57°	100.0 %	
Absorption correction	None	
Refinement method	Full-matrix least-squares on F^2	
Data / restraints / parameters	14110 / 105 / 562	
Goodness-of-fit on F^2	1.282	
Final R indices [I>2sigma(I)]	R1 = 0.0606, wR2 = 0.1667	
R indices (all data)	R1 = 0.0807, wR2 = 0.1813	
Largest diff. peak and hole	2.930 and -1.964 $e.Å^{-3}$	

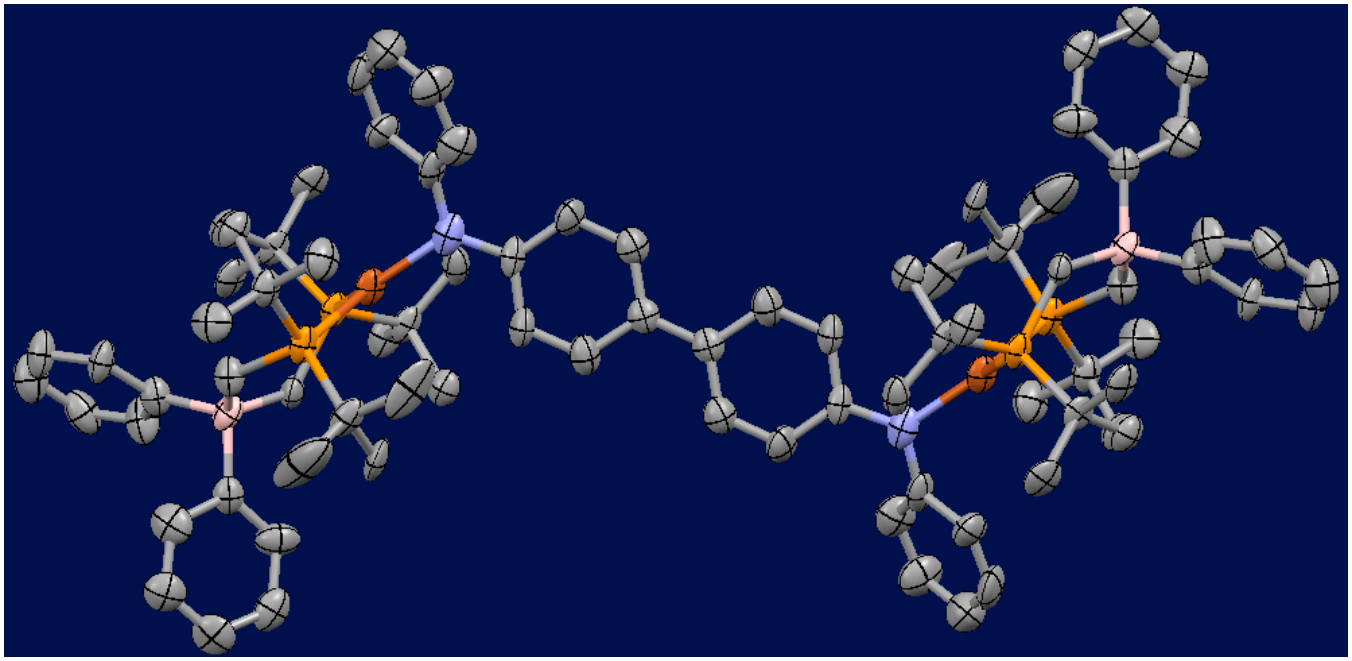

Figure S4. Thermal ellipsoid plot of **5** (50% ellipsoids, hydrogens omitted).

Table 3. Crystal data and structure refinement for **5**.

Empirical formula	$C_{42}H_{59}BCuNP_2$	
Formula weight	714.25	
Temperature	100(2) K	
Wavelength	0.71073 Å	
Crystal system	Monoclinic	
Space group	P2(1)/n	
Unit cell dimensions	a = 10.575(15) Å	α = 90°.
	b = 21.60(3) Å	β = 96.41(2)°.
	c = 16.50(2) Å	γ = 90°.
Volume	3745(9) $Å^3$	
Z	4	
Density (calculated)	1.297 Mg/m^3	
Absorption coefficient	0.702 mm^{-1}	
F(000)	1524	
Crystal size	0.45 x 0.10 x 0.10 mm^3	
Theta range for data collection	1.56 to 23.25°.	
Index ranges	-11<=h<=11, -24<=k<=24, -18<=l<=18	
Reflections collected	50483	
Independent reflections	5387 [R(int) = 0.3278]	
Completeness to theta = 23.25°	100.0 %	
Absorption correction	None	
Refinement method	Full-matrix least-squares on F^2	
Data / restraints / parameters	5387 / 0 / 436	
Goodness-of-fit on F^2	1.021	
Final R indices [I>2sigma(I)]	R1 = 0.1187, wR2 = 0.2839	
R indices (all data)	R1 = 0.2077, wR2 = 0.3511	
Largest diff. peak and hole	1.193 and -1.281 $e.Å^{-3}$	

UV-Vis measurements. Optical spectroscopy measurements were taken on a Cary 50 UV/Vis spectrophotometer using a 1-cm quartz cell sealed with a Teflon stopper

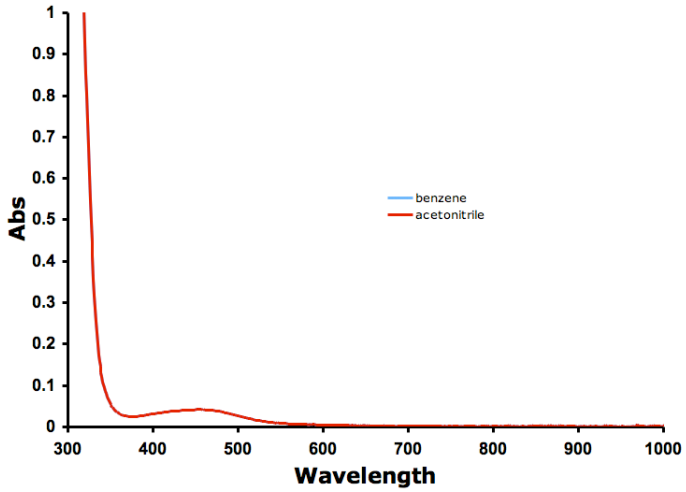

Figure S5. Optical spectra of **2** as equally concentrated benzene and acetonitrile solutions. Note: the blue line corresponding to the spectrum in benzene is invisible because of near-perfect overlap with the red line.

Self-exchange rate constant measurements. Self-exchange rate constant measurements were conducted using ^{1}H NMR line-broadening analysis.[3] Stock solutions of **1** in CD_3CN and **2** in C_6D_6 were prepared. The stock solution of **1** (400 μL) was placed in a J. Young NMR tube and the initial chemical shift (δ) and linewidth ($\nu_{1/2}$) of the tolyl methyl resonance were recorded. Increasing amounts of the stock solution of **2** were then added volumetrically, and the mole fraction of **2** (χ_2), concentration of **2** ([**2**]), and δ and $\nu_{1/2}$ for the tolyl methyl peak were recorded, each time locking, shimming, and referencing the ^{1}H NMR spectrum to the residual solvent peaks. A linear relationship between δ and χ_2 as well as between $\nu_{1/2}$ and χ_2 verified that electronic exchange between **1** and **2** was occurring in the fast-exchange regime. The plots for one data run are reproduced below. NMR parameters are as follows: sfrq = 300.080 MHz, acquisition time = 1.995 s, sweep width = 4506.5 Hz, pulse width = 7.0 ms, relaxation delay = 5 s, number of transients = 16, spectrometer temperature = 20.0 °C.

The relation between linewidth and the exchange rate (k) is given in eq 1, where W denotes linewidth, χ denotes mole fraction, C denotes concentration, and subscripts P, D, and PD denote paramagnet (i.e. **2**), diamagnet (i.e. **1**), and paramagnet/diamagnet mixtures, respectively.

$$W_{PD} = \chi_P W_P + \chi_D W_D + \frac{\chi_P \chi_D \left(4\pi(\delta\nu)^2\right)}{kC_{PD}} \qquad \text{(eq1)}$$

For all data points we measured (15 pts), the difference between W_{PD} and the sum $\chi_P W_P + \chi_D W_D$ was less than or equal to 1 Hz. In other words, the third term on the right-hand side of eq 1 was immeasurably small when considering the error associated with linewidth measurement. Because k is in the denominator of that term, it follows that k is too large to be measured accurately by this technique.

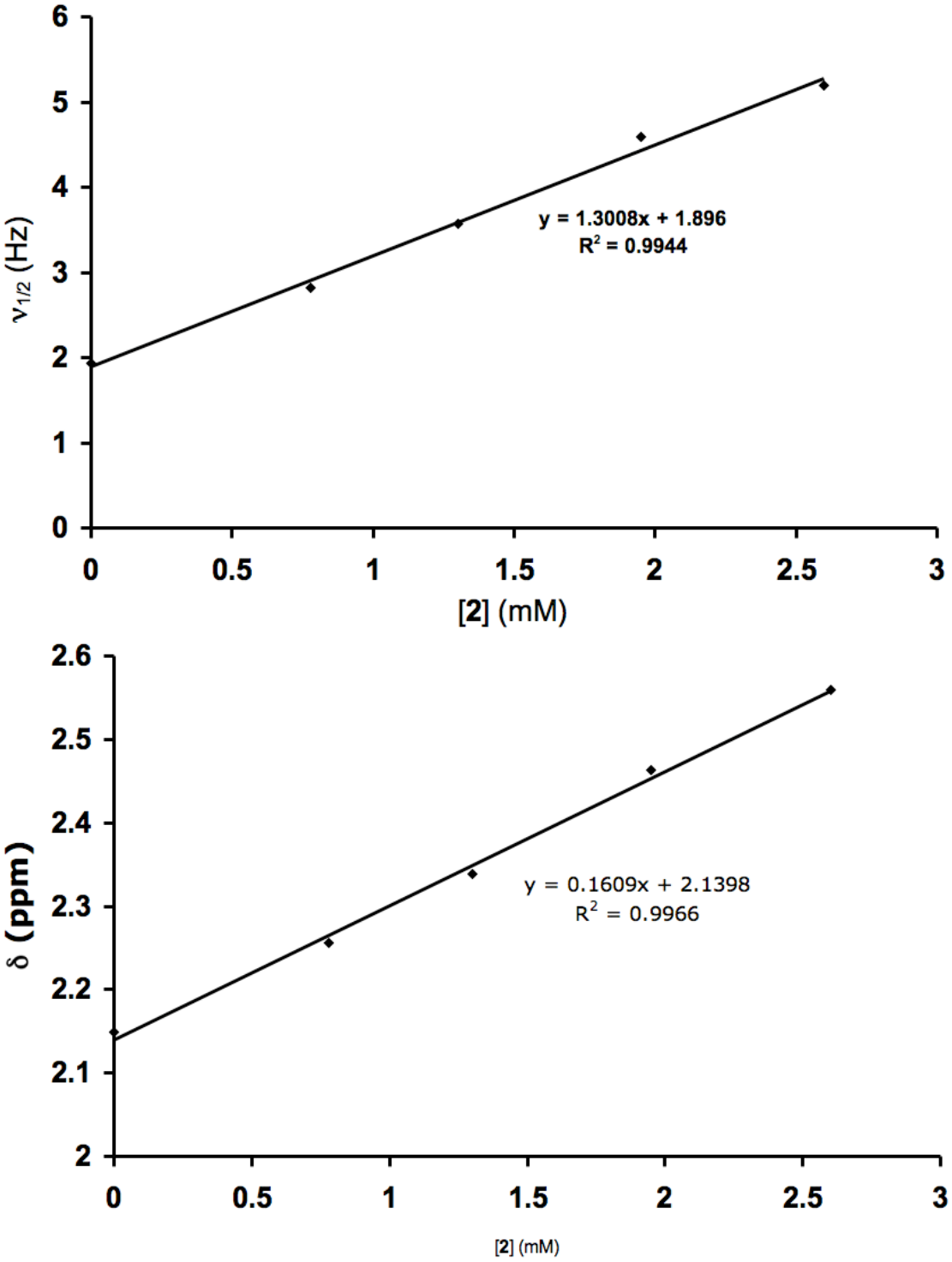

Figure S6. Plots of linewidth (*top*) and chemical shift (*bottom*) of the *p*-tolyl methyl ^{1}H NMR resonance in mixtures of **1** and **2** as a function of concentration of **2**.

Electronic Structure Calculations. Density functional calculations were carried out using the Gaussian03 suite.[4] The electronic structures of the computational models $\{(Ph_2BP^{tBu}{}_2]Cu^{I}(NTol)_2\}^{1-}$ and $\{(Ph_2BP^{tBu}{}_2]Cu^{II}(NTol)_2\}$ and their ionic fragments were calculated by employing a hybrid gradient-corrected density functional composed of 62% Becke nonlocal and Slater local density functional exchange[5a], 38% HF exact exchange, and 100% Perdew nonlocal and Vosko-Wilk-Nussair local density functional correlation[5b] functions. This hybrid functional (B(38)HFP86) has been shown to provide the most reasonable ground state electronic structures[6] for copper complexes among the most commonly used density functionals. Calculations were carried out using Gaussian type all electron basis sets[5c-d] with polarization and diffuse functions 6-311+G(d).[5e-g] We have utilized an ionic-fragment based approach[7] to achieve rapid wave function convergence and to compare and contrast the possibility of metal versus ligand centered localized as well as delocalized electronic structures. The molecular orbital contour plots were generated using GaussView 4.1[8].

Atomic coordinates for computational model {($Ph_2BP^{tBu}_2$]$Cu^{I}(NTol)_2$} (Z = -1; S = 0)

1	Cu	-8.1866	-9.1287	-10.8879	58	C	-5.6930	-10.9830	-12.1495
2	P	-6.2552	-9.2454	-12.0951	59	H	-4.8242	-10.9697	-12.6238
3	P	-8.1761	-10.9791	-9.6115	60	H	-6.3267	-11.4515	-12.7470
4	N	-9.4368	-7.5966	-11.0895	61	C	-6.4826	-11.6744	-9.5371
5	B	-5.4764	-11.9911	-10.8370	62	H	-6.5655	-12.5315	-9.0488
6	C	-4.8292	-8.2091	-11.4367	63	H	-5.9703	-11.0687	-8.9464
7	C	-5.0334	-6.7205	-11.7322	64	C	-3.9022	-11.9355	-10.3008
8	H	-4.3923	-6.1923	-11.2119	65	C	-3.5161	-11.8225	-8.9580
9	H	-4.8911	-6.5558	-12.6889	66	H	-4.1881	-11.7475	-8.2899
10	H	-5.9455	-6.4607	-11.4882	67	C	-2.1584	-11.8166	-8.5654
11	C	-3.4406	-8.6373	-11.9247	68	H	-1.9307	-11.7393	-7.6467
12	H	-3.3119	-9.5925	-11.7470	69	C	-1.1621	-11.9219	-9.5114
13	H	-3.3663	-8.4706	-12.8872	70	H	-0.2488	-11.9053	-9.2488
14	H	-2.7537	-8.1223	-11.4505	71	C	-1.5000	-12.0511	-10.8310
15	C	-4.8465	-8.3804	-9.9091	72	H	-0.8193	-12.1269	-11.4904
16	H	-5.6955	-8.0451	-9.5518	73	C	-2.8478	-12.0731	-11.2112
17	H	-4.7512	-9.3303	-9.6847	74	H	-3.0557	-12.1875	-12.1324
18	H	-4.1039	-7.8770	-9.5152	75	C	-5.6311	-13.5728	-11.3449
19	C	-6.5408	-8.8012	-13.9319	76	C	-5.7227	-13.9822	-12.6672
20	C	-5.2797	-8.7341	-14.7824	77	H	-5.7104	-13.3240	-13.3517
21	H	-4.7722	-7.9281	-14.5518	78	C	-5.8292	-15.3284	-13.0275
22	H	-4.7289	-9.5270	-14.6154	79	H	-5.9207	-15.5600	-13.9446
23	H	-5.5272	-8.7028	-15.7319	80	C	-5.8056	-16.3154	-12.0824
24	C	-7.3168	-7.4801	-14.0291	81	H	-5.8737	-17.2299	-12.3321
25	H	-7.5507	-7.3067	-14.9643	82	C	-5.6819	-15.9586	-10.7813
26	H	-8.1361	-7.5424	-13.4928	83	H	-5.6448	-16.6271	-10.1077
27	H	-6.7598	-6.7483	-13.6899	84	C	-5.6101	-14.6131	-10.4262
28	C	-7.4542	-9.8946	-14.5339	85	H	-5.5420	-14.3948	-9.5050
29	H	-6.9319	-10.7123	-14.6790	86	C	-8.8378	-6.3963	-10.7126
30	H	-8.1893	-10.0829	-13.9145	87	C	-8.1633	-6.3354	-9.5077
31	H	-7.8180	-9.5821	-15.3892	88	H	-8.2029	-7.0849	-8.9252
32	C	-8.5940	-10.6298	-7.7799	89	C	-7.4331	-5.2307	-9.1165
33	C	-9.8724	-9.7827	-7.7075	90	H	-6.9876	-5.2492	-8.2761
34	H	-9.8007	-9.0294	-8.3312	91	C	-7.3329	-4.1272	-9.8835
35	H	-10.6435	-10.3358	-7.9514	92	C	-8.0098	-4.1562	-11.1000
36	H	-9.9888	-9.4439	-6.7966	93	H	-7.9653	-3.3953	-11.6668
37	C	-7.4579	-9.8024	-7.2177	94	C	-8.7338	-5.2348	-11.5100
38	H	-6.6509	-10.3544	-7.1572	95	H	-9.1781	-5.2053	-12.3494
39	H	-7.2871	-9.0383	-7.8080	96	C	-6.5334	-2.9046	-9.4748
40	H	-7.7004	-9.4780	-6.3246	97	H	-5.5953	-3.1555	-9.3430
41	C	-8.7660	-11.8656	-6.9040	98	H	-6.5940	-2.2245	-10.1772
42	H	-8.7425	-11.6031	-5.9598	99	H	-6.8935	-2.5429	-8.6384
43	H	-9.6274	-12.2899	-7.1025	100	C	-10.5568	-7.6202	-11.9042
44	H	-8.0408	-12.4976	-7.0855	101	C	-11.4900	-6.5542	-12.0180
45	C	-9.3217	-12.3172	-10.2786	102	H	-11.3266	-5.7346	-11.5642
46	C	-9.0890	-12.3664	-11.7916	103	C	-12.6274	-6.6928	-12.7767
47	H	-9.7375	-12.9755	-12.2025	104	H	-13.2301	-5.9603	-12.8285
48	H	-9.1992	-11.4681	-12.1678	105	C	-12.9343	-7.8496	-13.4675
49	H	-8.1806	-12.6866	-11.9720	106	C	-12.0036	-8.8850	-13.3764
50	C	-10.8143	-11.9249	-10.0699	107	H	-12.1620	-9.6907	-13.8534
51	H	-11.3724	-12.4086	-10.7148	108	C	-10.8613	-8.7739	-12.6170
52	H	-11.0903	-12.1587	-9.1585	109	H	-10.2611	-9.5082	-12.5798
53	H	-10.9207	-10.9599	-10.2049	110	C	-14.2128	-7.9641	-14.3036
54	C	-9.0692	-13.7194	-9.7234	111	H	-14.0803	-7.5141	-15.1644
55	H	-8.1460	-13.9868	-9.9151	112	H	-14.4194	-8.9089	-14.4564
56	H	-9.2116	-13.7176	-8.7531	113	H	-14.9553	-7.5409	-13.8241
57	H	-9.6868	-14.3545	-10.1410					

Atomic coordinates for computational model {($Ph_2BP^{tBu}_2$]$Cu^{I}(NTol)_2$} (Z = 0; S = 1/2)

1	Cu	5.3601	13.6765	1.4458	58	C	4.9739	11.4397	3.9205
2	P	4.0281	12.1931	2.5569	59	H	4.3335	10.8571	4.4021
3	P	7.0568	14.1047	2.9102	60	H	5.6281	10.8342	3.4921
4	N	4.9865	14.3683	-0.2961	61	C	6.4734	13.7211	4.5958
5	B	5.8257	12.2616	5.1098	62	H	7.2422	13.9000	5.1938
6	C	2.4383	12.8821	3.2785	63	H	5.7928	14.4069	4.8082
7	C	2.8373	14.1694	4.0293	64	C	4.8638	12.5793	6.4145
8	H	2.0374	14.5835	4.4143	65	C	4.7639	13.8035	7.0809
9	H	3.2596	14.7944	3.4044	66	H	5.2921	14.5311	6.7737
10	H	3.4671	13.9474	4.7458	67	C	3.9234	14.0033	8.1761
11	C	1.7611	11.9362	4.2783	68	H	3.8970	14.8532	8.5996
12	H	0.9652	12.3712	4.6521	69	C	3.1344	12.9876	8.6497
13	H	2.3866	11.7237	5.0026	70	H	2.5316	13.1364	9.3682
14	H	1.4988	11.1105	3.8195	71	C	3.2385	11.7382	8.0556
15	C	1.4244	13.2688	2.1904	72	H	2.7243	11.0108	8.3860
16	H	0.9734	12.4627	1.8627	73	C	4.0925	11.5489	6.9786
17	H	1.8925	13.7070	1.4480	74	H	4.1589	10.6788	6.6043
18	H	0.7610	13.8836	2.5667	75	C	6.9794	11.2407	5.7220
19	C	3.6850	10.7472	1.3719	76	C	7.8177	11.6843	6.7608
20	C	3.0306	9.5370	2.0295	77	H	7.7248	12.5805	7.0631
21	H	2.9664	8.8066	1.3797	78	C	8.7683	10.8849	7.3653
22	H	2.1313	9.7795	2.3385	79	H	9.3093	11.2348	8.0649
23	H	3.5709	9.2481	2.7940	80	C	8.9341	9.5702	6.9513
24	C	5.0496	10.3240	0.8040	81	H	9.5877	9.0127	7.3555
25	H	5.6182	9.9937	1.5318	82	C	8.1307	9.0928	5.9409
26	H	5.4799	11.0942	0.3771	83	H	8.2338	8.1968	5.6454
27	H	4.9215	9.6128	0.1405	84	C	7.1699	9.9061	5.3474
28	C	2.8262	11.2035	0.1692	85	H	6.6229	9.5408	4.6612
29	H	2.8775	10.5317	-0.5428	86	C	4.2482	15.5233	-0.5155
30	H	3.1640	12.0605	-0.1658	87	C	3.4370	16.0284	0.5084
31	H	1.8941	11.3084	0.4536	88	H	3.3633	15.5433	1.3208
32	C	7.3404	15.9888	2.9163	89	C	2.7444	17.2062	0.3702
33	C	8.4749	16.4552	3.8360	90	H	2.1890	17.5070	1.0790
34	H	8.5138	17.4351	3.8361	91	C	2.8419	17.9689	-0.7937
35	H	9.3274	16.0943	3.5126	92	C	3.6389	17.4702	-1.8069
36	H	8.3095	16.1335	4.7471	93	H	3.7142	17.9681	-2.6128
37	C	6.0298	16.6316	3.3868	94	C	4.3276	16.2859	-1.7015
38	H	5.8949	16.4393	4.3386	95	H	4.8573	15.9798	-2.4286
39	H	5.2822	16.2643	2.8698	96	C	2.1280	19.2863	-0.9037
40	H	6.0744	17.6019	3.2530	97	H	2.2862	19.6703	-1.7917
41	C	7.5939	16.5021	1.4833	98	H	2.4657	19.8992	-0.2180
42	H	7.5651	17.4809	1.4775	99	H	1.1661	19.1487	-0.7731
43	H	6.9029	16.1515	0.8838	100	C	5.3809	13.5981	-1.4169
44	H	8.4743	16.1989	1.1798	101	C	4.5015	13.3261	-2.4748
45	C	8.6824	13.2000	2.6541	102	H	3.6368	13.7185	-2.4847
46	C	9.5628	13.1583	3.9129	103	C	4.8918	12.4922	-3.4993
47	H	9.0936	12.6737	4.6239	104	H	4.2824	12.3107	-4.2052
48	H	9.7507	14.0733	4.2101	105	C	6.1469	11.9117	-3.5307
49	H	10.4063	12.7015	3.7078	106	C	7.0232	12.1799	-2.4882
50	C	8.3207	11.7539	2.2769	107	H	7.8912	11.7956	-2.4894
51	H	9.1413	11.2413	2.1254	108	C	6.6361	13.0041	-1.4478
52	H	7.7808	11.7547	1.4589	109	H	7.2439	13.1675	-0.7368
53	H	7.8088	11.3443	3.0044	110	C	6.5455	11.0059	-4.6944
54	C	9.4971	13.7988	1.5009	111	H	5.7928	10.4238	-4.9285
55	H	9.8430	14.6767	1.7670	112	H	7.3147	10.4581	-4.4336
56	H	8.9223	13.9000	0.7128	113	H	6.7843	11.5569	-5.4693
57	H	10.2449	13.2034	1.2861					

Details of XAS Data Collection. The copper K-, phosphorus K-, and copper L-edge XAS measurements were carried out at beamlines 7-3, 6-2, and 10-1, respectively, of Stanford Synchrotron Radiation Laboratory under storage ring (SPEAR3) conditions of 3 GeV energy and 100-80 mA current. BL7-3 is a 20-pole, 2 T Wiggler beam line equipped with a Si(220) downward reflecting, double-crystal monochromator. Data was collected in the energy range of 8660-9690 eV using an unfocused beam. The samples were placed in a liquid He cryostat and about 11 K temperature was maintained throughout the measurements. The beam intensity was maximized at 9685 eV. The data was collected in transmission mode. BL6-2 is a 56-pole, 0.9 T Wiggler beam line with a liquid-nitrogen-cooled, Si(111) double-crystal monochromator. P K-edge spectra were collected in the energy range of 2120- 2250 eV using an unfocused beam in a He-purged beam path at room temperature and a 3-element Lytle fluorescence detector. The beam line was optimized at 2320 eV. BL10-1 has a 30-pole 1.45 T Wiggler insertion device with 6 m spherical grating monochromator. The samples were placed in a vacuum chamber with operating pressures below 10^{-5} torr. The incident beam energy was scanned between 925 and 955 eV and beam line optics were optimized at 920 eV. Data collection was carried out in electron yield mode by a channeltron detector with 300 V accelerating potential.

The samples were ground and pasted onto a contaminant-free Kapton tape from Shercon or carbon tape from Specs CertiPrep in a glovebox with sub parts per million oxygen and moisture levels. Samples for transmission measurements were diluted in and ground together with boronitride to minimize incident beam absorption. Samples were protected by a thin polypropylene window (Specs CertiPrep) from exposure to air during sample mounting and change. Sample holders for Cu L-edge measurements were mounted in a He-purged glove-bag tightly wrapped around the vacuum chamber. The sensitivity of the finely dispersed samples on the sample cells were tested by exposing them immediately after measurements for about 30 s to air followed by a repeated data collection. Even in the most sensitive samples, such as CuCl we only observed negligible change in the spectral feature intensities or energy positions.

The incident photon energy was scanned in 0.5 eV steps outside the rising edge regions for each edges where the step-size was 0.1 eV. At least five scans were averaged to obtain a good signal-to-noise ratio. Radiation damage was observed at the Cu L-edge for the radical complex $\{(Ph_2BP^{tBu}{}_2)Cu^{II}(NTol_2)\}$, which was corrected for by estimating the rate of change from two scans of three with 1 s and 0.5 s dwell times for two different sample positions. The incident photon energy was calibrated to the spectra of copper foil at the Cu K-edge (first inflection point at 8979 eV), difluorocopper(II) at the Cu L_3- and L_2-edges (white line positions at 930.5 and 950.5 eV, respectively), and triphenylphosphineoxide at the P K-edge (maximum of pre-edge feature at 2147.5 eV).

The averaged raw data was background subtracted using a second order polynomial fit to the approximately 30 eV energy range before any spectral feature and normalized with a second order spline function above the edge jump at 9200, 980, 2890, and 2190 eV for the Cu K-, Cu L-, Cl K-, and P K-edges, respectively. Due to the different number of absorbers per molecule the Cl K-edge spectra had to be renormalized in order to compare the pre-edge features of $CuCl_2$ and Cs_2CuCl_4 samples. The pre-edge features at the P K-, Cl K-, and Cu L-edges were fitted using the edg_fit program of EXAFSPAK.[9] Fitting parameters and representatives fits are given in Figure S9. Fits to the pre-edge features at the Cl K-edge (Figure S9A) were used to determine the Cl 3p covalency in anhydrous $CuCl_2$ using the reference spectra and pre-edge fits for D_{2d} Cs_2CuCl_4.[10] Due to the complementarity of orbital coefficients, 100% less the above Cl 3p covalency gave the amount of Cu 3d character in the probed unoccupied, frontier orbitals of the $CuCl_2$. This provided a Cu 2p→3d transition dipole moment, which was used to quantitate the Cu L-edge pre-edge features (Figure S9B) of the $\{(Ph_2BP^{tBu}{}_2)Cu^{II}(NTol_2)\}$ sample. Due to the lack of good standards the P character represented by the pre-edge feature at the P K-edge (Figure S9C) was estimated from results of electronic structure calculations.

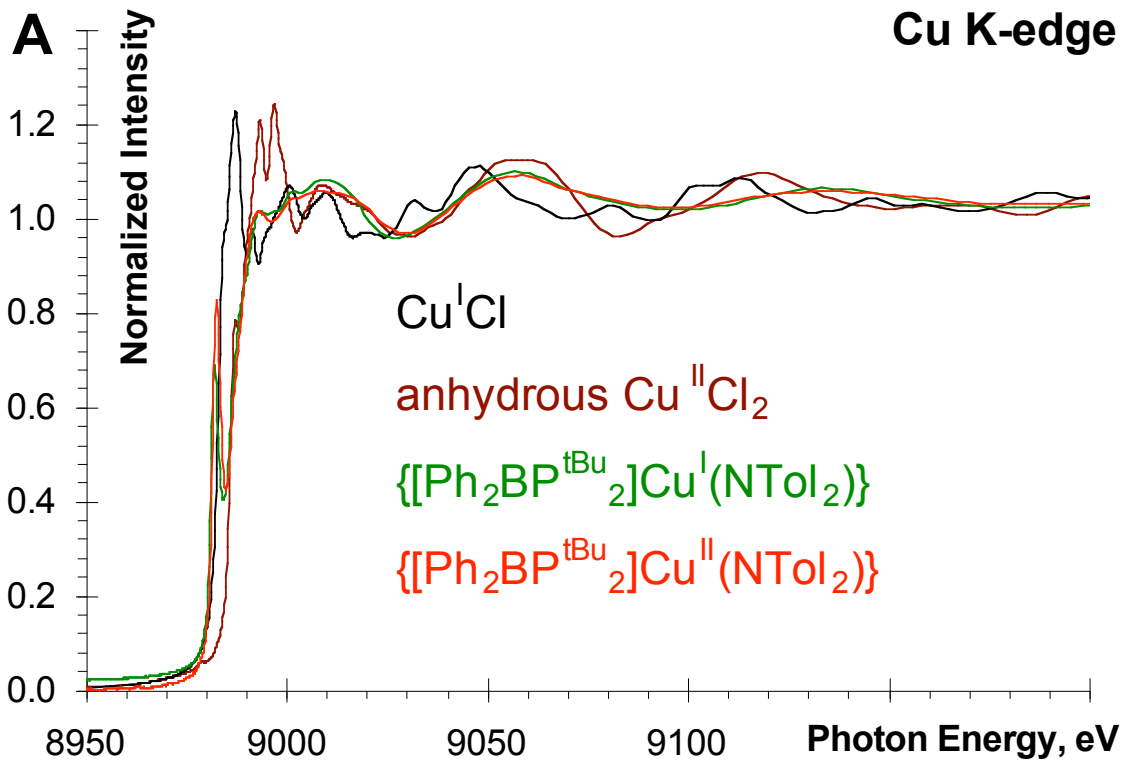

Figure S7A. Background corrected and normalized Cu K-edge spectra for CuCl (black), anhydrous $CuCl_2$ (brown), 1(green) and 2(red)

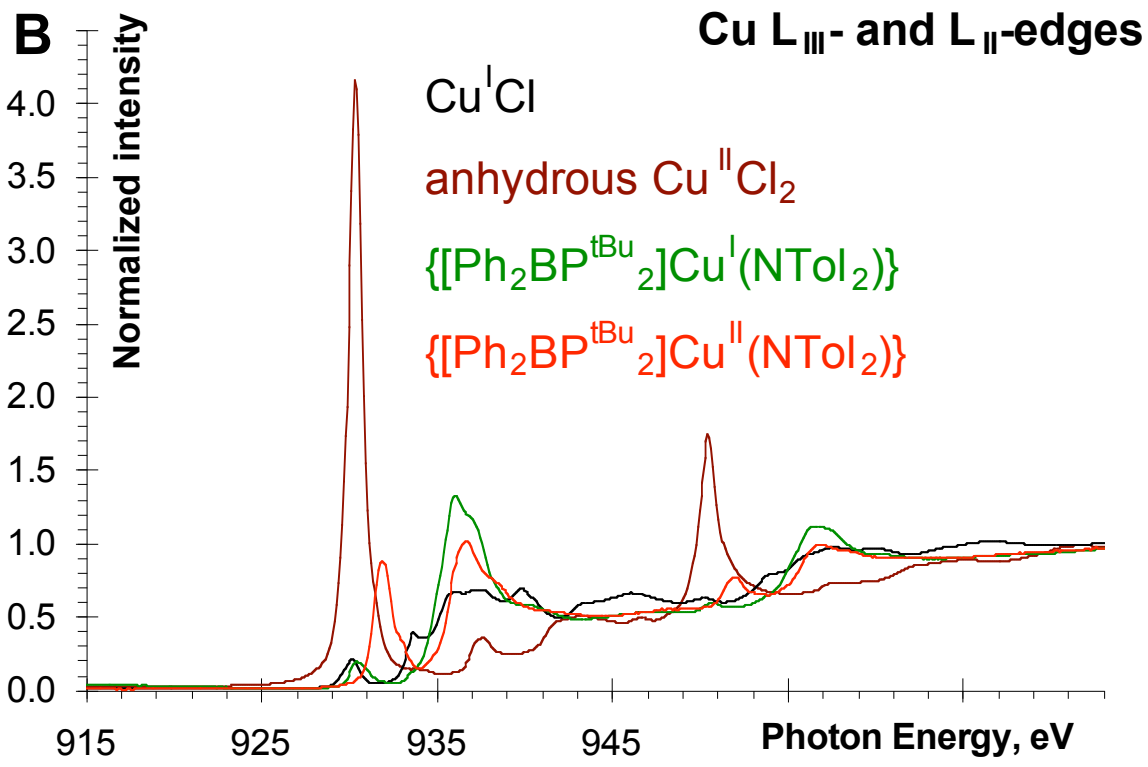

Figure S7B. Background corrected and normalized Cu L-edge spectra for CuCl (black), anhydrous $CuCl_2$ (brown), 1(green) and 2(red)

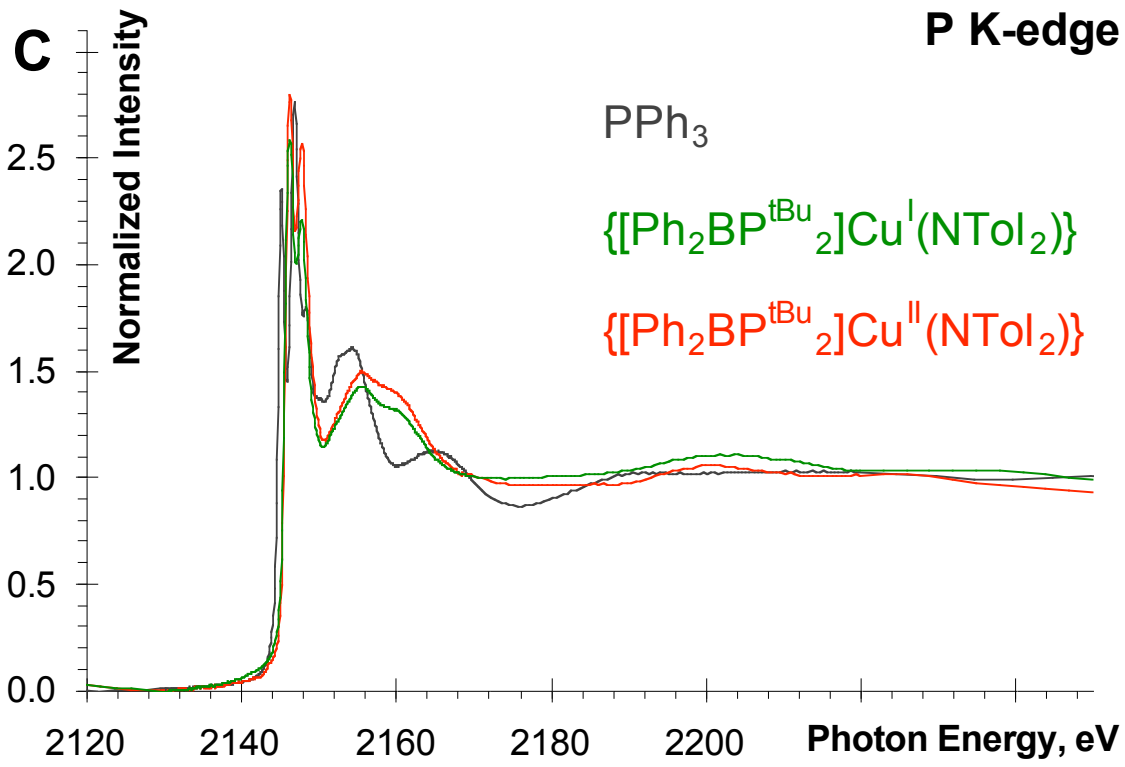

Figure S7C. Background corrected and normalized P K-edge spectra for PPh_3 (black), 1(green) and 2(red)

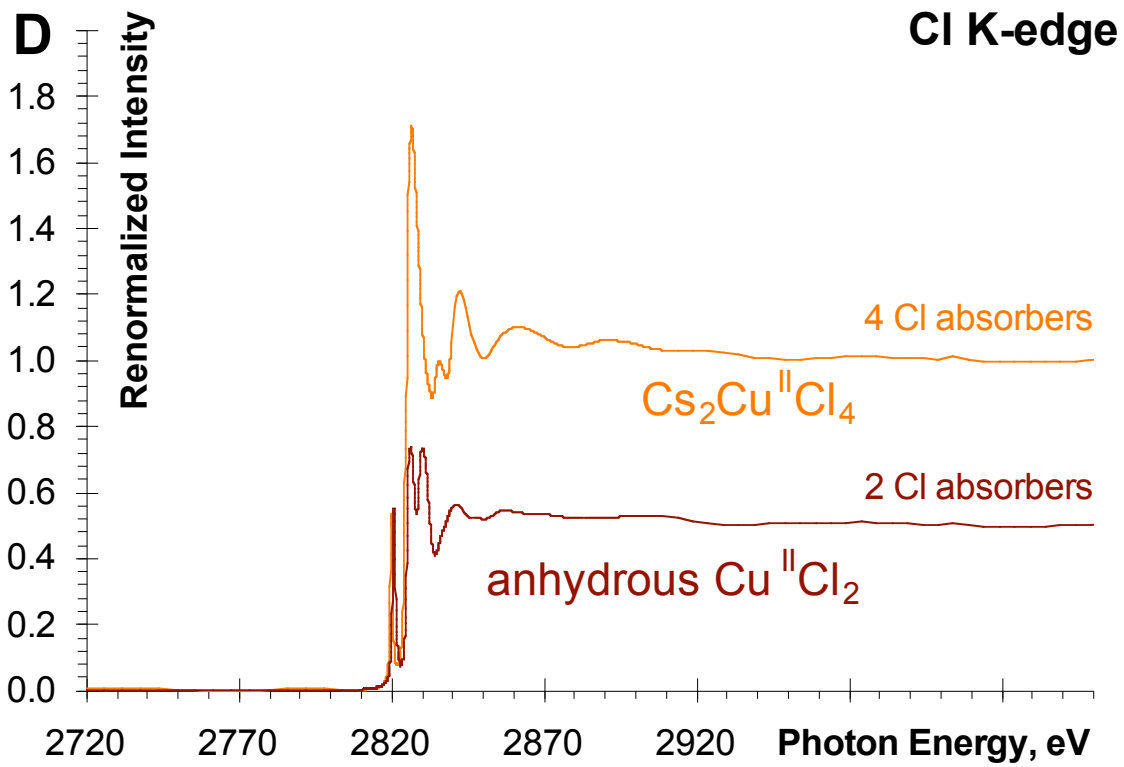

Figure S7D. Background corrected and renormalized Cl K-edge spectra for D_{2d} $Cs_2Cu^{II}Cl_4$ (orange) and anhydrous $Cu^{II}Cl_2$

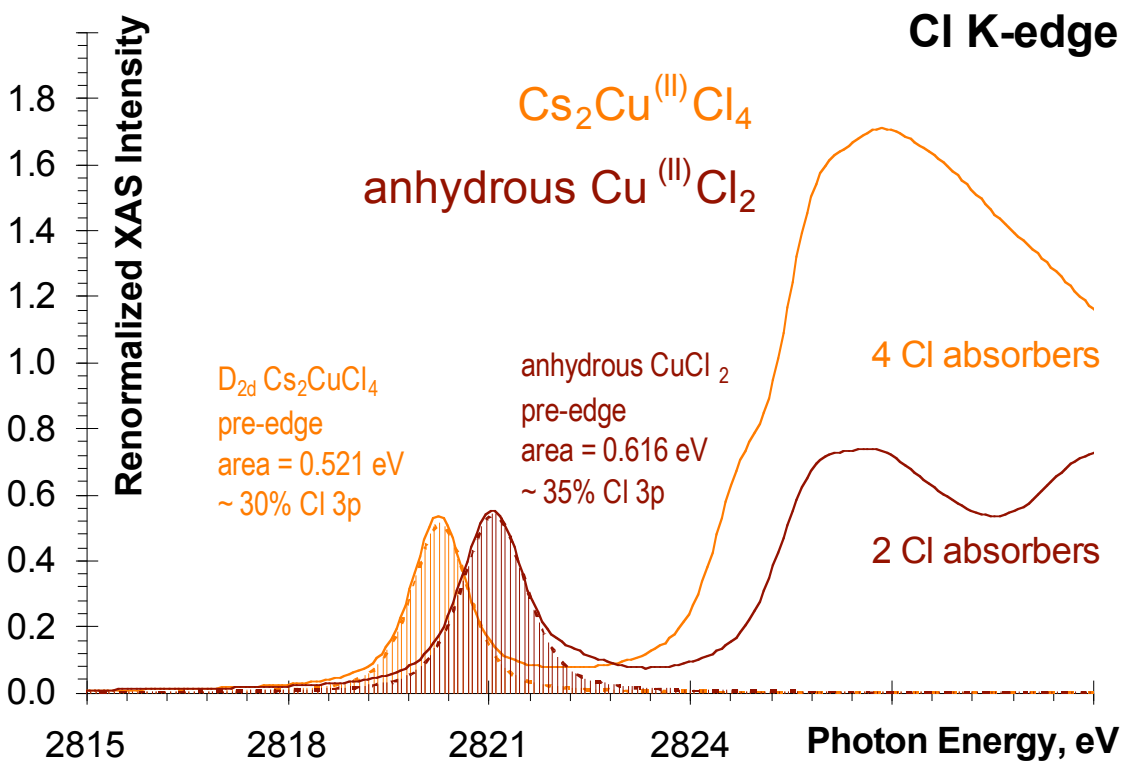

Figure S8. Fitted Cl K-edge XANES spectra for D_{2d} $Cs_2Cu^{II}Cl_4$ (orange) and anhydrous $Cu^{II}Cl_2$ to generate transition dipole integrals for quantifying the Cu L-edge pre-edge features

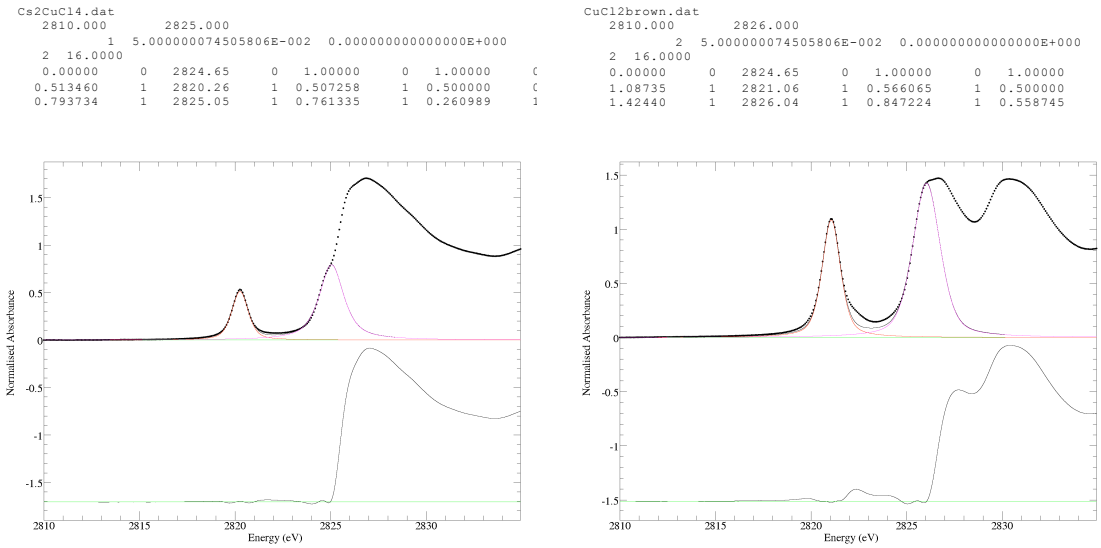

Figure S9A. Representative fits to the pre-edge features at the Cl K-edge spectra

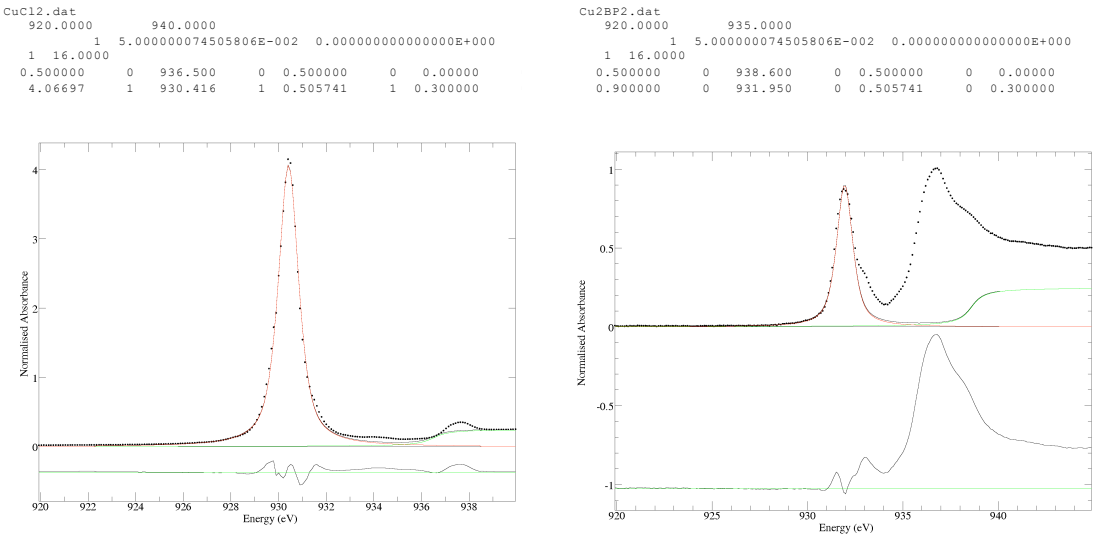

Figure S9B. Representative fits to the pre-edge features at the Cu L_3-edge spectra

```
Cu1BP2.dat
  2140.  2150.
 1  0.0500000007  0.
   2  16.0000
   1.00000      0   2148.50      1   1.17571      1  0.869465
   2.04091      1   2146.29      1  0.544170      1   1.00000
   2.29790      1   2147.81      1   1.06906      1  0.308965
```

```
Cu2BP2.dat
  2140.  2150.
 2  0.0500000007  0.
   3  16.0000
   1.00000      0   2148.80      1   1.17571      0  0.869465
   1.59780      0   2146.45      0  0.544170      0  0.500000
   1.89920      0   2147.85      0   1.06906      0  0.308965
  0.780000      0   2145.93      0  0.450000      0  0.500000
```

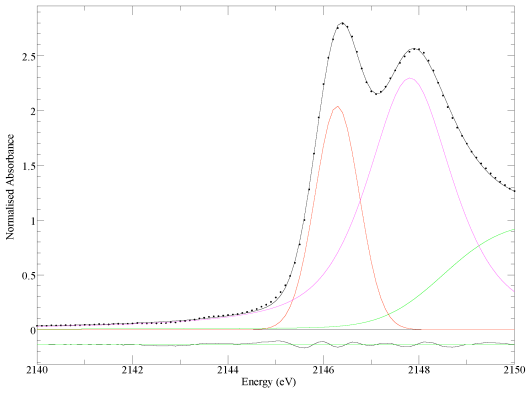

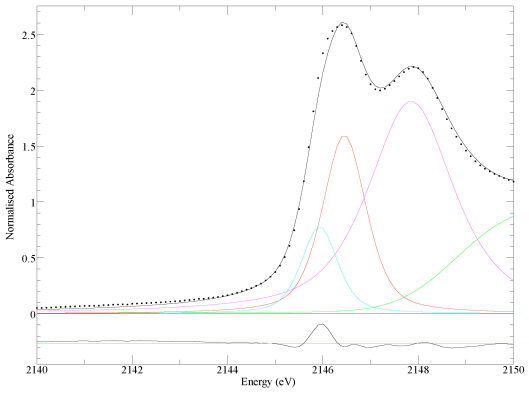

Figure S9C. Representative fits to the pre-edge features at the P K-edge spectra

EPR measurements. EPR spectra were obtained at the National Biomedical EPR center in Milwaukee using Varian E-9 and E-109 spectrometers operating at 9.188 GHz (X-band), 3.392 GHz (S-band), and 35.100 GHz (Q-band). The low frequency 3.3 GHz (S-band) spectrometer is based on the loop-gap resonator designed by Froncisz and Hyde.[11] The Q-band bridge was modified with the addition of a GaAs field-effect transistor signal amplifier and low-noise Gunn diode oscillator.[12] Microwave frequencies were measured with an EIP model 331 counter. Spectra were recorded in a frozen glass of dichloromethane/toluene at 123 K (S- and Q-band) or 77 K (X-band). Spectra are reported from 4 scans with time constant 0.128 s, modulation amplitude 5 G, and microwave power 30 dB (Q-band) or 16 dB (X- and S-band). The second derivative of the spectra was obtained by using SUMSPC92, a data manipulation program available upon request from the National Biomedical EPR Center. The second derivative spectra emphasize sharp lines. A 1% argument was used to obtain the second derivative spectrum.

EPR simulations. EPR simulations were carried out using the program W95EPR,[13] and using the following logic. Six lines dominate the S- and X-band spectra, but there are several shoulders on the six lines (Figure 4, main text). In all three spectra, sharp high-field lines are evident. (The spectra depicted in Figure 4 are aligned with these high-field lines.) A line on the low-field side is well resolved in the S- and X-band spectra and is a shoulder at Q-band. The outer lines of the spectra appear to be hill-shaped, not S-shaped, and are assigned to g_z. Assigning these lines as purely Cu lines leads to unsatisfactory simulations (see below, Figure S11). One way to get a six-line pattern is to have A^{Cu} approximately equal to A^{P} for two equivalent phosphorus donor atoms, resulting in lines with intensities 1:3:4:4:3:1. Experimentally, if the outer lines are set to intensity 1, then the measured intensities of the adjacent lines are close to 3. The rest of the spectra are fit with g and A values as follows (same parameters for all three fields): g_x, g_y, g_z = 2.008, 2.008, 2.030; $A^{Cu}{}_x$, $A^{Cu}{}_y$, $A^{Cu}{}_z$ = 34, 34, 170 MHz; $A^{P}{}_x$, $A^{P}{}_y$, $A^{P}{}_z$ = 148, 148, 173 MHz; $A^{N}{}_x$, $A^{N}{}_y$, $A^{N}{}_z$ = 24, 100, 24 MHz. Linewidths of W_x, W_y, W_z = 10 G, 10 G, 20 G were used for S- and X-band simulations, and 10 G, 10 G, 30 G for Q-band simulations. These

simulations are overlaid with experimental spectra in Figure S10. Figure S12 shows simulations in which all other parameters are held constant and A^{N}_{y} is varied as indicated.

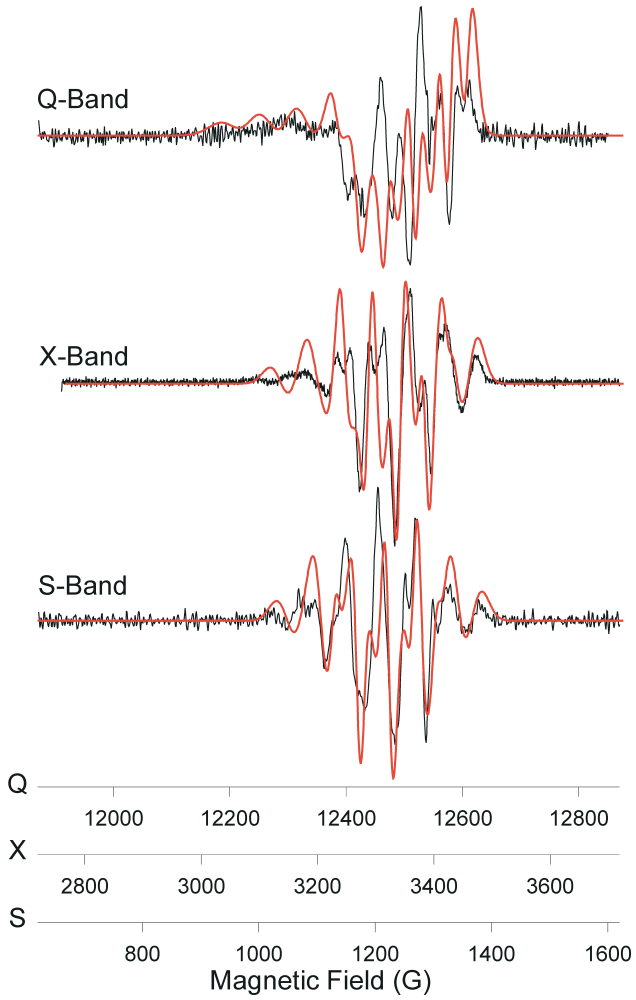

Figure S10. Experimental (*black*) and simulated (*red*) second derivative EPR spectra of **2** at Q-, X-, and S-bands.

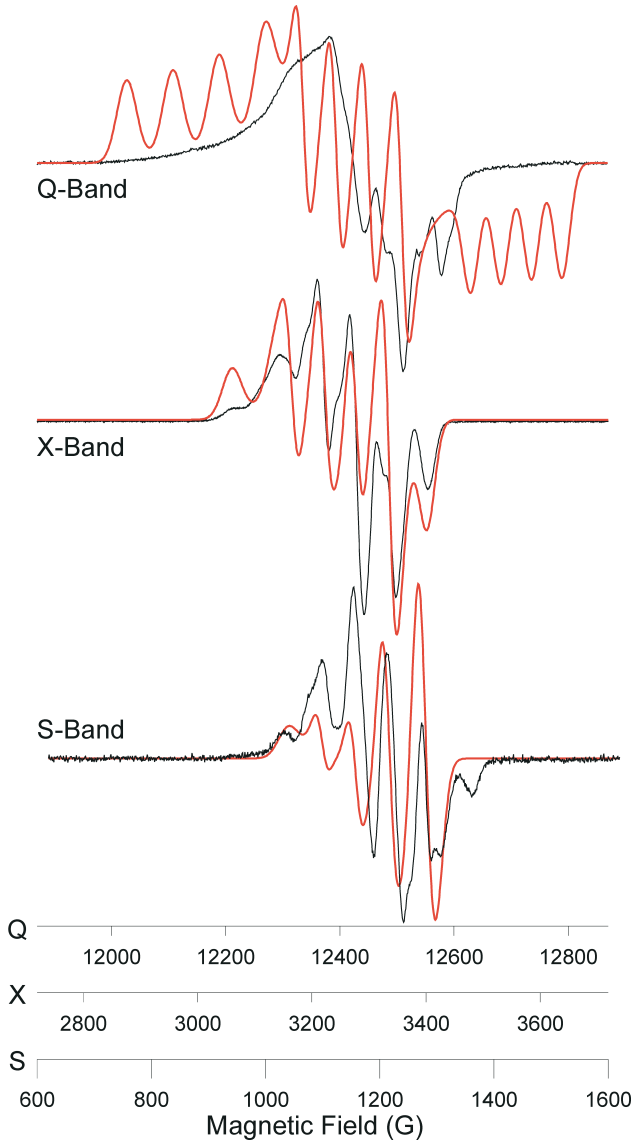

Figure S11. Experimental (*black*) and simulated (*red*) EPR spectra of **2** resulting from assigning outer lines as deriving purely from Cu.

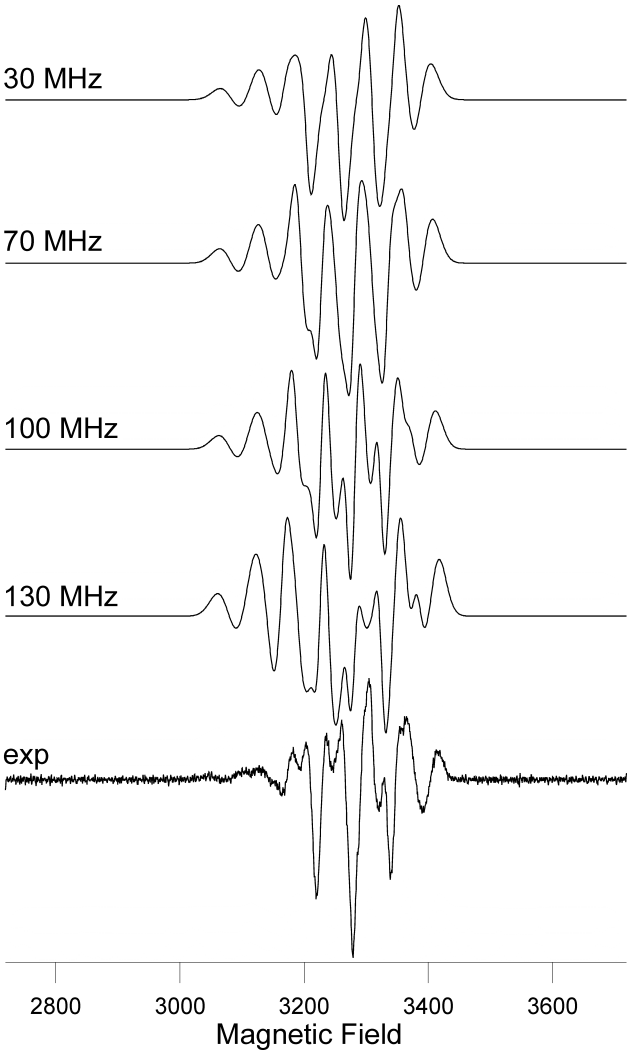

Figure S12. Simulated second derivative X-band spectra of **2** resulting from maintaining all other simulation parameters while varying A^{N}_{y} as indicated.

Determination of k_H/k_D

A dilute solution of **3** in C_6H_6 (~70 μM) was placed in a cuvette and stopped with a rubber septum. UV-Vis scans were obtained every 1 min, and after the first scan either neat Bu_3SnH or neat Bu_3SnD (> 25 equiv per Cu) was added to the cuvette through the septum by syringe. An example of the resulting decomposition of **3** as monitored by UV-Vis is reproduced below. A plot of $|\ln(A_{365})|$ vs t revealed linear relationships in both cases, and the ratio of the slopes provided the kinetic isotope effect (see plot below). The average of three trials is reported.

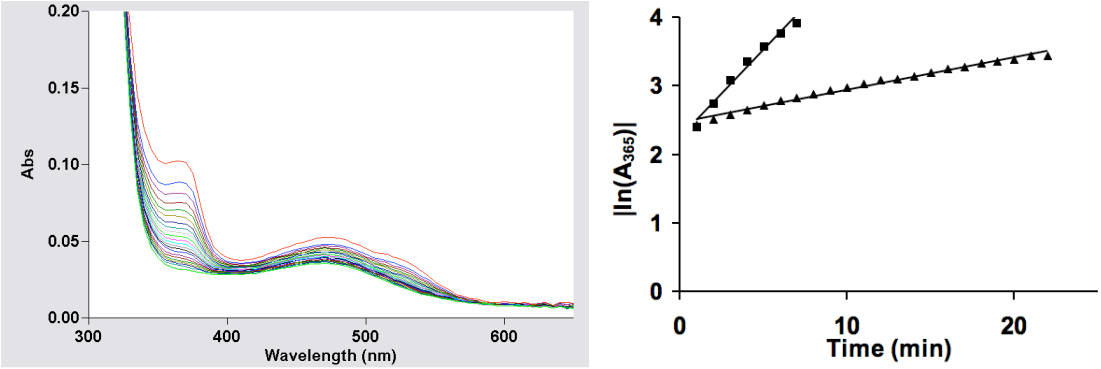

Figure S13. (*left*) Example of UV-Vis spectroscopy used to monitor the decomposition of **3**, in this case with the addition of ~25 equiv Bu_3SnD. (*right*) Plot of $|\ln(A_{365})|$ vs time for Bu_3SnH (squares) and Bu_3SnD (triangles).

References

[1] Mankad, N. P.; Peters, J. C. *Chem. Commun.* **2008**, 1061.
[2] Chavez, I.; *J. Organomet. Chem.* **2000**, *601*, 126.
[3] (a) Goodwin, J. A.; Stanbury, D. M.; Wilson, L. J.; Eigenbrot, C. W.; Scheidt, W. R. *J. Am. Chem. Soc.* **1987**, *109*, 2979. (b) Pulliam, E. J.; McMillin, D. R. *Inorg. Chem.* **1984**, *23*, 1172. (c) McConnell, H. M.; Berger, S. B. *J. Chem. Phys.* **1957**, *27*, 230.
[4] Frisch, M. J.; Trucks, G. W.; Schlegel, H. B.; Scuseria, G. E.; Robb, M. A.; Cheeseman, J. R.; Montgomery, J. A. J.; Vreven, T.; Kudin, K. N.; Burant, J. C.; Millam, J. M.; Iyengar, S. S.; Tomasi, J.; Barone, V.; Mennucci, B.; Cossi, M.; Scalmani, G.; Rega, N.; Petersson, G. A.; Nakatsuji, H.; Hada, M.; Ehara, M.; Toyota, K.; Fukuda, R.; Hasegawa, J.; Ishida, M.; Nakajima, T.; Honda, Y.; Kitao, O.; Nakai, H.; Klene, M.; Li, X.; Knox, J. E.; Hratchian, H. P.; Cross, J. B.; Adamo, C.; Jaramillo, J.; Gomperts, R.; Stratmann, R. E.; Yazyev, O.; Austin, A. J.; Cammi, R.; Pomelli, C.; Ochterski, J. W.; Ayala, P. Y.; Morokuma, K.; Voth, G. A.; Salvador, P.; Dannenberg, J. J.; Zakrzewski, V. G.; Dapprich, S.; Daniels, A. D.; Strain, M. C.; Farkas, O.; Malick, D. K.; Rabuck, A. D.; Raghavachari, K.; Foresman, J. B.; Ortiz, J. V.; Cui, Q.; Baboul, A. G.; Clifford, S.; Cioslowski, J.; Stefanov, B. B.; Liu, G.; Liashenko, A.; Piskorz, P.; Komaromi, I.; Martin, R. L.; Fox, D. J.; Keith, T.; Al-Laham, M. A.; Peng, C. Y.; Nanayakkara, A.; Challacombe, M.; Gill, P. M. W.; Johnson, B.; Chen, W.; Wong, M. W.; Gonzalez, C.; Pople, J. A. Gaussian03, Rev. C02; Gaussian, Inc.: Pittsburgh PA, 2004.
[5] a) Feller, D., *J. Comp. Chem.* **1996**, 17, 1571-1586. b) Schuchardt, K.L., Didier, B.T., Elsethagen, T., Sun, L., Gurumoorthi, V., Chase, J., Li, J., and Windus, T.L. *J. Chem. Inf. Model.* **2007**, 47, 1045-1052. c) Becke, A. D. *Phys. Rev. A: Gen. Phys.* **1988**, 38, 3098. d) Perdew, J. P. *Phys. Rev. B: Condens. Matter Mater. Phys.* **1986**, 33, 8822. e) Wachters, A. J. H. *J. Chem. Phys.* **1970**, 52, 1033; f) Hay, P. J. *J. Chem. Phys.* **1977**, 66, 4377. g) Raghavachari, K. Trucks, G. W. *J. Chem. Phys.* **1989**, 91, 1062.
[6] Szilagyi, R. K.; Metz, M.; Solomon, E. I., *J. Chem. Phys. A* **2002**, 106, 2994-3007.
[7] Szilagyi, R. K.; Winslow, M. *J. Comput. Chem.* **2006**, 27, 1385.
[8] GaussView, Version 4.1; Roy Dennington II, Todd Keith and John Millam, Semichem, Inc., Shawnee Mission, KS, 2007.
[9] EXAFSPAK: A suite of computer Programs for Analysis of X-ray Absorption Spectra. G.N. George, I.J. Pickering, June 2000 (http://www-ssrl.slac.stanford.edu/~george/exafspak/)
[10] Hedman, B.; Hodgson, K.O.; Solomon, E.I. *J. Am. Chem. Soc.* **1992**, 112, 1643-1645
[11] Froncisz, W.; Hyde, J. S. *J. Magn. Reson.* **1982**, *47*, 515.
[12] Hyde, J. S.; Newton, M. E.; Strangeway, R. A.; Camenisch, T. G.; Froncisz, W. *Rev. Sci. Instrum.* **1991**, *62*, 2969.
[13] Neese, F. *QCPE Bull.* **1995**, *15*, 5.